BIOCHEMISTRY
including biophysical chemistry & molecular biology

Article

pubs.acs.org/biochemistry

Cross-Seeding of Fibrils from Two Types of Insulin Induces New Amyloid Strains

Weronika Surmacz-Chwedoruk,[†,‡] Hanna Nieznańska,[§] Sławomir Wójcik,[∥] and Wojciech Dzwolak*[,∥]

[†]Institute of Biotechnology and Antibiotics, Staroscinska 5, 02-516 Warsaw, Poland

[‡]Institute of High Pressure Physics, Polish Academy of Sciences, Sokolowska 29/37, 01-142 Warsaw, Poland

[§]Nencki Institute of Experimental Biology, Polish Academy of Sciences, Pasteura 3, 02-093 Warsaw, Poland

[∥]Department of Chemistry, University of Warsaw, Pasteura 1, 02-093 Warsaw, Poland

Supporting Information

ABSTRACT: The irreversibility and autocatalytic character of amyloidogenesis and the polymorphism of amyloid fibrils underlie the phenomenon of self-propagating strains, wherein the mother seed, rather than the seeding environment, determines the properties of daughter fibrils. Here we study the formation of amyloid fibrils from bovine insulin and the recombinant Lys^{B31}-Arg^{B32} human insulin analog. The two polypeptides are similar enough to cross-seed but, upon spontaneous aggregation, form amyloid fibrils with distinct spectral features in the infrared amide I′ band region. When bovine insulin is cross-seeded with the analog amyloid (and vice versa), the shape, absorption maximum, and even fine fingerprint features of the amide I′ band are passed from the mother to daughter fibrils with a high degree of fidelity. Although the differences in primary structure between bovine insulin and the Lys^{B31}-Arg^{B32} analog of human insulin lie outside of the polypeptide's critical amyloidogenic regions, they affect the secondary structure of fibrils, possibly the formation of intermolecular salt bridges, and the susceptibility to dissection and denaturation with dimethyl sulfoxide (DMSO). All these phenotypic features of mother fibrils are imprinted in daughter amyloid upon cross-seeding. Analysis of noncooperative DMSO-induced denaturation of daughter fibrils suggests that the self-propagating polymorphism underlying the emergence of new amyloid strains is encoded on the level of secondary structure. Our findings have been discussed in the context of polymorphism of fibrils, amyloid strains, and possible implications for mechanisms of amyloidogenesis.

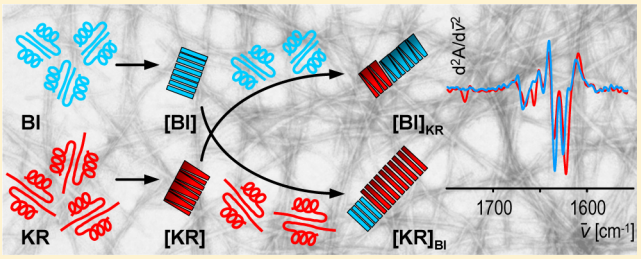

Misfolding of protein molecules, their subsequent aggregation, and the formation of β-sheet-rich amyloid fibrils are intimately connected to the etiology of several degenerative disorders, including Alzheimer's disease, Parkinson's disease, and diabetes mellitus type II.[1] As the formation of amyloid fibrils is thought to represent a common property of proteins as polymers (polyamides), the process may also be induced in vitro in benign proteins, synthetic peptides, or even polymerized α-amino acids.[2] Proteins, which in the native "precursor" state may be very different in terms of size, structure, and biological function, often form almost indistinguishable amyloid fibrils sharing similar β-sheet content, nanometric diameter, and elongated unbranched morphology. However, the apparent similarity and structural simplicity of amyloid fibrils from different proteins conceal the complexity of a different nature. First, the similarities of fibrils from various amyloidogenic proteins and peptides hold only on a rather low-resolution level of structural analysis that is currently accessible in most amyloid studies.[3] Second, unlike formation of a correctly folded native state in which the end structure is unequivocally encoded in the amino acid sequence, aggregation of misfolded protein molecules with an identical primary structure may lead to distinct fibrils. The resulting polymorphism is a violation of the Anfinsen's dogma stipulating that the thermodynamic control of the folding process (i.e., the native state corresponds to the minimum of the free energy) determines its unambiguity.[4] Nevertheless, a wealth of new experimental evidence of polymorphism of amyloid fibrils from diverse proteins (e.g., refs 5−10) and the idea that at least some of these amyloid structural variants may represent lower-than-the-native-state free energy level even under in vivo conditions[11,12] have recently led to a paradigm shift in this field.[13−16] The relative thermodynamic metastability of singly dispersed protein molecules is the driving force of autocatalytic self-assembly of amyloid fibrils. That, coupled to the irreversibility of amyloidogenesis and polymorphism of fibrils, evokes a particular type of non-Anfinsenian behavior: self-propagating polymorphism observed upon seeding of certain amyloidogenic proteins with preformed structural variants of fibrils (assembled from covalently identical molecules) in which structural features of mother fibrils (the seed) are passed on to

Received: August 23, 2012
Revised: November 4, 2012
Published: November 5, 2012

   dx.doi.org/10.1021/bi301144d | *Biochemistry* 2012, 51, 9460−9469

the daughter amyloid regardless of environmental biases favoring alternative types of fibrils. An alternative term, conformational memory,[8] has been coined to reflect the profoundly conformational-transition-pathway-dependent nature of protein amyloidogenesis. The most important clinical implications of the self-propagating polymorphism of amyloid fibrils are as follows: (i) a single type of unmutated amyloidogenic precursor protein may convert into distinct, also in terms of biological activity (i.e., toxicity), types of fibrils, and (ii) a local conformational fluctuation at early stages of aggregation may spread, through the autocatalytic loops, to large quantities of the misfolded protein. Such kinetically stable self-propagating structural variants of amyloid fibrils formed from a single unmutated type of protein are often called strains, by analogy to mammalian and yeast "prion strains".[17] Today, it is generally accepted that self-propagating variations in amyloid structure underlie the existence of different strain phenotypes.[18−26]

Undertaking efforts to elucidate strain-type polymorphism of amyloid fibrils is crucial for gaining deeper insights into obscure structural factors ruling the toxicity (or infectivity) of protein aggregates in Alzheimer's and Creutzfeld-Jakob's diseases and for finding new effective therapeutic strategies. Because strain-dependent fibrillation patterns can be reproduced in vitro in benign and more accessible proteins, using amyloidogenic models such as insulin has become common and led to many important findings. While fibrillation of insulin in vivo does not seem to pose any major clinical problem,[27] the hormone readily aggregates also in vitro, producing a variety of structural forms, including spherulites,[28] twisted or flat protofibrils,[29,30] or larger superstructures of many laterally aligned fibrils[31] that may also exhibit fascinating chiroptical properties, as we have shown in our earlier works.[32−34]

One of the most interesting aspects of polymorphism of insulin fibrils emerged when it was discovered that in the presence of certain diluted cosolvents such as ethanol or acetic acid insulin forms distinct and kinetically stable conformational variants of fibrils with characteristic spectral fingerprints in the amide I′ vibrational region.[35] We employed two types of insulin fibrils formed spontaneously either in an entirely aqueous environment (type I) or in the presence of diluted ethanol (type II) in a cross-seeding experiment in which the phenotype of the mother seed (determined by its spectral FT-IR characteristics,[9] and morphological traits[36]) was competing with the environment's bias favoring an alternative type. As the daughter fibrils revealed spectral and morphological features of mother fibrils (rather than of those forming de novo in the absence of cross-seeding), we proposed that this behavior mimics the essential features of prion strains, implying thereby that strain-dependent polymorphism may be common among amyloidogenic proteins.[9,36,37] We used FT-IR spectroscopy as the main tool permitting detection of tiny variations between different amyloid strains. In fact, infrared absorption[8−10,38−43] and Raman scattering[29,44−46] are two vibrational spectroscopic methods often employed to probe conformation of amyloid fibrils. Certain vibrational bands, especially the amide I band (marked I′ for a fully deuterated peptide backbone), are sensitive not only to the type of conformation but also to its fine structural details: mutual orientation of strands within a β-sheet, its local twist, and strength of inter-β-strand hydrogen bonding.[47,48]

This FT-IR study is focused on cross-seeding behavior between two types of insulin: from bovine pancreas (BI) and the Lys^{B31}-Arg^{B32} analog of human recombinant insulin (KR), whose differences in primary structure are located outside of insulin's main amyloidogenic regions, according to Eisenberg et al.[49−51] Our primary interest was to see if variations in the amino acid sequence beyond critical amyloidogenic regions can induce new strains and whether conformational memory effects could determine the stability and disaggregation pathways of amyloid strains.

MATERIALS AND METHODS

Samples. BI (insulin from bovine pancreas) was from Sigma-Aldrich, while HI and its analogs (GEKR, GKR, GR, and KR) were manufactured by the Institute of Biotechnology and Antibiotics using recombinant DNA technology.[67] D_2O ("99.8 atom % D" grade) was from ARMAR Chemicals, and deuterium chloride (35 wt % DCl solution in D_2O, 99 atom % D) was from Sigma-Aldrich.

Mother amyloid fibrils were obtained through a quiescent incubation of 1 wt % insulin solutions in 0.1 M NaCl in D_2O [pH* 1.9 adjusted with diluted DCl (where pH* is the pH-meter readout uncorrected for isotopic effects)] at 65 °C for 48 h. Subsequently, insoluble aggregates of amyloid fibrils were subjected to FT-IR/TEM analysis or, after sonication, used as seeds to induce daughter amyloid fibrils.

For seeding experiments, sonicated mother fibrils were added to freshly prepared 1 wt % insulin solutions in 0.1 M NaCl in D_2O (pH* 1.9) at a 100:1 native insulin:insulin fibril mass ratio. To prevent competitive de novo formation of amyloid nuclei, the temperature of the following incubation phase was set at 37 °C.

FT-IR Spectroscopy. For FT-IR measurements, a CaF_2 transmission cell equipped with a 0.05 mm Teflon spacer was used. The temperature in the cell was controlled through an external water-circuit connected to a programmable thermostat. All FT-IR spectra were recorded on a Nicolet NEXUS FT-IR spectrometer equipped with a liquid nitrogen-cooled MCT detector. Typically, for a single spectrum, 256 interferograms at 2 cm^{-1} resolution were co-added. During measurements, the sample chamber was continuously purged with dry CO_2-depleted air. All insulin spectra were corrected by subtracting the correct amount of buffer (D_2O, or a proper D_2O/DMSO solution) and water vapor spectra prior to being baseline-corrected and then normalized by the integrated intensity of the amide I′ band. Data processing, including calculations of second-derivative spectra (Savitzky−Golay), was performed using GRAMS (ThermoNicolet). Values of the center of spectral mass used in Figure 1C were calculated according to the formula

$$\langle \bar{\nu} \rangle = \frac{\sum_{i=1}^{N} \bar{\nu}_i A_i}{\sum_{i=1}^{N} A_i}$$

where A_i is the absorption at wavenumber ν_i.[52] The summation was conducted for wavenumbers in the range between 1700 and 1590 cm^{-1}. All further details have been described previously.[9,53]

CD Spectroscopy. Insulin samples in acidified D_2O-based solutions (as prepared for FT-IR measurements) were further diluted 100 times with 0.01 M hydrochloric acid prior to far-UV CD measurements. All CD spectra of native and aggregated insulin samples were collected at 25 °C on a Jasco J-815 S spectropolarimeter using 1 mm quartz cuvettes, as specified in our previous work.[34]

dx.doi.org/10.1021/bi301144d | Biochemistry 2012, 51, 9460−9469

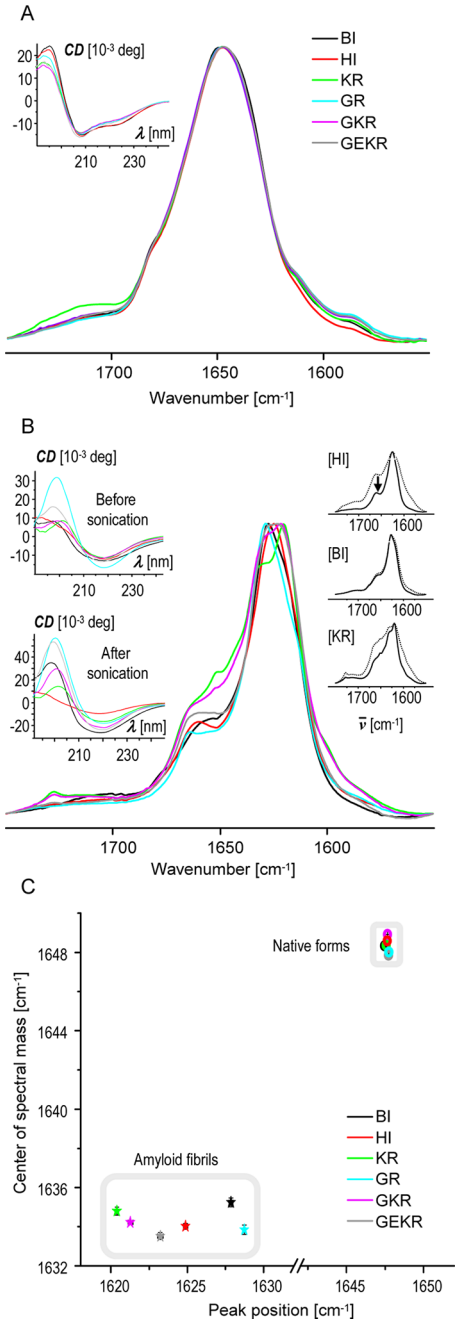

Figure 1. (A) Amide I′ vibrational region of FT-IR spectra of fully deuterated insulin samples in their native states at pH* 1.9 and 25 °C. The inset shows the corresponding far-UV CD spectra. (B) Amide I′ bands of corresponding amyloid fibrils (obtained through spontaneous aggregation of fully deuterated insulin samples). Spectra were collected after a brief sonication of completely aggregated samples. Corresponding far-UV CD spectra of amyloid samples before and after sonication are shown in the left inset. The right inset shows infrared spectra of [HI], [BI], and [KR] fibrils before (···) and after (—) sonication. (C) Scattergraph of the amide I′ band positions and corresponding centers of spectral mass calculated for the infrared bands from panels A and B. Plotted are mean values obtained from averaging measuremnts of five independent samples of each native or amyloid type of insulin. The exact values and corresponding standard deviations are provided as Supporting Information.

Kinetic Measurements of ThT Fluorescence. For kinetic experiments, a Fluoroskan Ascent FL fluorometer equipped with a pair of λ_{ex} = 440 nm/λ_{em} = 485 nm optical filters and 96-well black microplates was used. Sample conditions were the same as those for FT-IR measurements except that ThT was added to a final concentration of 20 μM. Aggregation of insulin samples was monitored by probing the intensity of ThT fluorescence excited at 440 nm. Kinetic experiments were conducted at 40 °C with gentle agitation at 420 rpm. To assess the reproducibility of aggregation kinetics, six microplate wells were filled with 170 μL portions of each sample for parallel measurements. All further details were described previously.[33]

Transmission Electron Microscopy. For TEM, 400 mesh copper grids (Sigma-Aldrich) covered with collodion (SPI Supplies, West Chester, PA) and carbon were used. A 10 μL sample (1 mg/mL) was applied to a grid for 40 s and then negatively stained for 25 s with 2% (w/v) uranyl acetate (SPI Supplies). Grids were dried at room temperature and examined using a JEM 1400 electron microscope (JEOL Co.) with a high-resolution digital camera (CCD MORADA, SiS-Olympus).

DMSO-Induced Denaturation. Briefly, sonicated fibrils were centrifuged at 13000 rpm and subsequently resuspended in a proper DMSO/D_2O solution so that the final insulin concentration was maintained at 0.3 wt % while DMSO:D_2O ratios varied. After a brief incubation and equilibration, spectroscopic measurements followed. FT-IR data were collected as specified earlier. For fluorescence measurements, samples were additionally stained with 3 μM ThT. Emission spectra were collected using AMINCO Bowman Series 2 luminescence spectrometer (λ_{ex} = 450 nm) and 2 mm quartz cuvettes. Measurements of static light scattering at 350 nm were taken using the same cuvette and spectrometer setup in the absence of ThT. All further experimental details were the same as specified previously.[33,54]

RESULTS AND DISCUSSION

Even minor substitutions in a protein's amino acid sequence may affect the stability and conformation of the native state. Structures of both HI and BI are quite similar, while the modifications of HI analogs studied in this work lie mostly in C-terminal parts of insulin's chains (Table 1) and as such are not expected to affect significantly the native conformation. This was corroborated by FT-IR and far-UV CD spectra of fully deuterated insulin samples acquired before and after spontaneous aggregation (Figure 1). A very high level of similarity between secondary structures of all six types of insulin may be inferred from the almost identical infrared spectra in the amide I′ band region shown in Figure 1A. This is further confirmed by the lack of any clear differences in the corresponding far-UV CD spectra (inset in Figure 1A). The almost symmetrical amide I′ band centered around 1648 cm^{-1} and the double CD minima at 208 and 222 nm are spectroscopic manifestations of α-helical structure that is the main secondary structural component of the native insulin conformation. As the conversion of native insulin into amyloid fibrils entails refolding of α-helices into stacked β-sheets, the process is accompanied by pronounced changes in both infrared absorption and optical activity. FT-IR and CD spectra of fibrils obtained from all the six types of insulin through spontaneous aggregation of acidified samples of the native forms are shown in Figure 1B. As some freshly prepared fibrils were visibly inhomogeneous (with larger particles corresponding to spherulites[28] and other higher-order structures precipitating from the viscous gel), the samples were briefly sonicated prior to the acquisition of spectra. Unexpectedly, the ultrasound treatment affected spectra of

dx.doi.org/10.1021/bi301144d | Biochemistry 2012, 51, 9460−9469

Table 1. Amino Acid Sequences of the A and B Chains of Different Types of Insulin[a]

type of insulin	symbol	sequence
bovine insulin	BI	A chain, GIVEQCCASVCSLYQLENYCN
		B chain, FVNQHLCGSHLVEALYLVCGERGFFYTPKA
human insulin	HI	A chain, GIVEQCCTSICSLYQLENYCN
		B chain, FVNQHLCGSHLVEALYLVCGERGFFYTPKT
Gly^{A22}-Glu^{B3}-Lys^{B31}-Arg^{B32} human insulin analog	GEKR	A chain, GIVEQCCTSICSLYQLENYCNG
		B chain, FVEQHLCGSHLVEALYLVCGERGFFYTPKTKR
Gly^{A22}-Lys^{B31}-Arg^{B32} human insulin analog	GKR	A chain, GIVEQCCTSICSLYQLENYCNG
		B chain, FVNQHLCGSHLVEALYLVCGERGFFYTPKTKR
Gly^{A22}-Arg^{B31} human insulin analog	GR	A chain, GIVEQCCTSICSLYQLENYCNG
		B chain, FVNQHLCGSHLVEALYLVCGERGFFYTPKTR
Lys^{B31}-Arg^{B32} human insulin analog	KR	A chain, GIVEQCCTSICSLYQLENYCN
		B chain, FVNQHLCGSHLVEALYLVCGERGFFYTPKTKR

[a]Underlined are insulin's two amyloidogenic regions (according to refs 50 and 51).

insulin aggregates, as well. The amide I′ band became narrower and CD signals more intense (right and left insets in Figure 1B, respectively). An overlap with broad spectral components originating from insulin molecules not fully converted into orderly β-sheets is a likely cause of the initial "bloated" appearance of amide I′ bands, which disappeared after sonication (right inset in Figure 1B). Given the high insulin concentration used in the fibrillation protocol, and the absence of agitation, it seems likely that a portion of protein molecules missed the opportunity to dock and integrate with tips of elongating fibrils and became trapped in the viscous matrix of grown amyloid afterward (i.e., until the sonication released them and allowed them to bind to fibrils' ends). That the case of [BI] is quite different (right inset of Figure 1B) could be explained by a more accessible secondary nucleation pathway (nucleation on surfaces of existing fibrils);[31,56,57] i.e., contact interactions even with surfaces of [BI] fibrils could promote a complete conversion of trapped molecules into mature amyloid without sonication.

The red shift below 1630 cm^{-1} and the narrowing of the amide I′ band reflect the formation of β-sheet-rich fibrils.[53] Interestingly, unlike for the native states, fibrils from different types of insulin reveal distinct spectral features in terms of the absorption maximum, the shape of the amide I′ peak, and other fine details such as the tiny spikes appearing in spectra of [KR] and [GKR] at 1651 and 1728 cm^{-1}. The latter bands cannot be assigned to vibrations of amino acid side chains introduced along with the amino acid modifications of KR and GKR because of the lack thereof of the corresponding spectra of native forms of the two analogs (apart from the fact that of all the substituting side chains only arginine could give a weak signal around 1608 cm^{-1}).[58] Hence, the subtle differences in FT-IR spectra of fibrils from six types of insulin should be primarily attributed to conformational variations. Figure 1C summarizes the effects of the sequence modifications on the amide I′ bands (of native and fibrillar forms of insulin). Plotting the center of spectral mass (defined in Materials and Methods) against the peak's position accentuates conformational differences between insulin forms. On the basis of that, we have selected two types of fibrils ([BI] and [KR]) whose infrared features turned out to be sufficiently distinct to track possible conformational memory effects (Figure 1C). The tiny discrepancies in the amino acid sequences between the two polypeptides [two in the A chain and three in the B chain (Table 1)] lie outside of insulin's "core" amyloidogenic segments[50,51] and thus were not expected to prevent cross-seeding. Docking interactions between the amyloid seed and "incoming" monomers are highly specific, which generally requires that an active template be formed through self-assembly of the same protein as the one that is seeded or one very similar.[60] However, there are many examples of effective seeding with heterologous fibrils.[61−63] Insulin is particularly promiscuous in this respect, as it can be seeded with fibrils from either its individual A and B chains[64] or insulin isomers with scrambled disulfide bridges.[45] Even amorphous aggregates of a single-chain analog of insulin exhibit the capacity to trigger aggregation of HI.[45] We have confirmed that cross-seeding between [KR] and [BI] is very effective (and mutual) using ThT fluorescence (Figure 2). Time traces of fluorescence intensity exhibit no lag phases, while in the absence of seeds but under otherwise identical experimental conditions, ThT emission remains at the "zero" level for the first 5 and 10 h for KR and BI, respectively (data not shown). There are several interesting aspects of the data reported in Figure 2 that lie beyond the scope of this paper and will not be analyzed here in detail. For example, the low fluorescence plateau for BI seeded homologously with [BI] (Figure 2 A) may originate either from different properties of surface ThT-binding moieties of resulting $[BI]_{BI}$ fibrils (dumping quantum yield of the fluorophore) or from the superstructural organization of daughter fibrils restricting access to ThT-binding sites. The quasi-sigmoidal shape of time traces in Figure 2D suggests a pronounced acceleration of fibrillation that is typically associated with secondary nucleation events but could also be caused by the greater brittleness of $[KR]_{BI}$ fibrils. This would lead to rapid multiplication of fibrils' ends upon agitation.[23]

Confirming that [BI] and [KR] fibrils can efficiently catalyze each other's growth was a starting point for conducting the key experiment of this study, which was a comparison of properties of daughter fibrils obtained through cross-seeding of both types of insulin fibrils. To minimize de novo formation of competing amyloid nuclei, cross-seeding was conducted in quiescent samples thermostated at 37 °C. Absorption and second-derivative FT-IR spectra of fibrils formed through spontaneous (unseeded) aggregation at 65 °C and through seeding with homologous fibrils via cross-seeding at 37 °C are shown in Figure 3. Clearly, the spectra of mother amyloid and homologous daughter fibrils are, within the accuracy of the method, indistinguishable. This holds true for the amide I′ band's absorption maximum (1628 cm^{-1} for $[BI]/[BI]_{BI}$ and 1620 cm^{-1} for $[KR]/[KR]_{KR}$) and tiny spectral features at 1728 and 1651 cm^{-1} visible only in the spectra of $[KR]/[KR]_{KR}$

dx.doi.org/10.1021/bi301144d | Biochemistry 2012, 51, 9460−9469

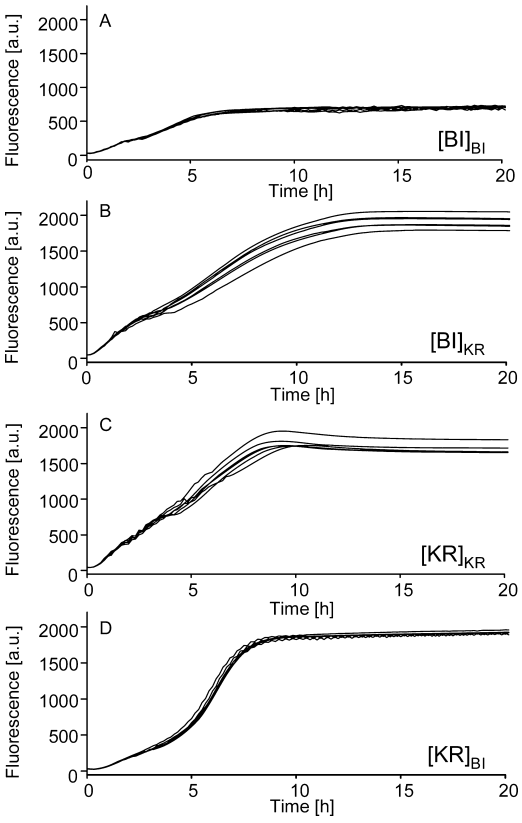

Figure 2. Kinetics of seeded aggregation of BI and KR at 40 °C monitored by ThT fluorescence. Aggregation of native BI in the presence of 1 wt % [BI] amyloid (A) or [KR] amyloid (B) and of native KR seeded with 1 wt % [KR] amyloid (C) or [BI] amyloid (D). The multiple lines correspond to several wells monitored simultaneously under identical sample and temperature conditions.

fibrils. Importantly, all the spectral traits of mother fibrils appear to be reproduced in daughter fibrils upon cross-seeding, which proves the occurrence of a conformational memory effect. Also, the presence of the 1728/1651 cm^{-1} bands in the spectrum of $[BI]_{KR}$ fibrils wherein approximately 99% of the total mass of fibrils corresponds to BI molecules lends further credence to the argument that they do not reflect the amino acid composition of the seeded polypeptide (overlapping vibrational bands of KR side chains) but a more subtle effect controlled by the seed's conformation. The 1728 cm^{-1} band lies outside of the amide I′ wavenumber range. Likewise, the 1651 cm^{-1} peak is unlikely to originate from backbone amide I′ vibrations for different reasons: this frequency range corresponds to helical or disordered structures that, even if residually present in the aggregates, have much larger bandwidths, making it overlapped and unresolved from the main amide I′ band's background (unlike the amyloid core's β-sheet known to give rise to narrow signals but at lower wavenumbers). The two peaks are likely to stem from amino acid side chains, glutamic acid (1728 cm^{-1}) and asparagine/glutamine (1651 cm^{-1}),[58] that are abundant in insulin (Table 1) and whose structural surroundings in [BI] and [KR] might be very different. The 1728 cm^{-1} band corresponds to stretching vibrations of a deuterated carboxyl group (-COOD) that could be either of a Glu side chain or of the main chains' C-termini. In spite of the pH* of the samples being well below the pK_a of either type of carboxyl group[65] and the same concentration of -COOD groups in BI and KR, the 1728 cm^{-1} band disappears from the spectra of [BI], $[BI]_{BI}$, and

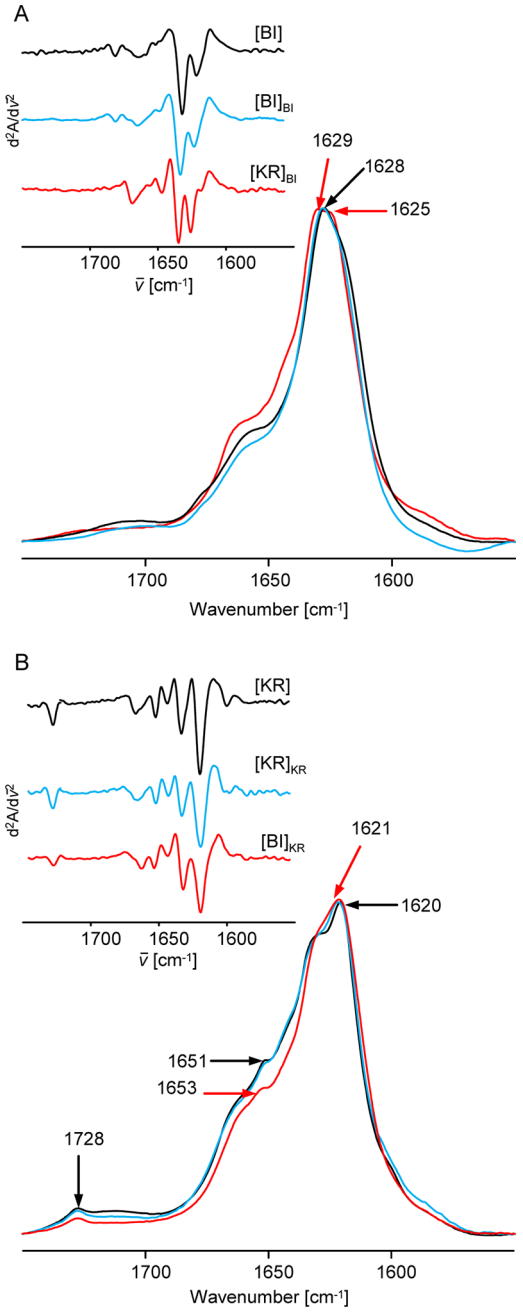

Figure 3. Amide I′ spectral region of fully deuterated insulin fibrils obtained through spontaneous aggregation [[BI] (A) and [KR] (B) (black lines)], seeded with homologous fibrils [$[BI]_{BI}$ (A) and $[KR]_{KR}$ (B) (blue lines)], or cross-seeded [$[KR]_{BI}$ (A) and $[BI]_{KR}$ (B) (red lines)]. Corresponding second-derivative spectra are shown in the insets.

$[KR]_{BI}$ (Figure 3). We propose that the most plausible explanation for the vanishing 1728 cm^{-1} band is ionization of carboxyls, e.g., through salt bridge interactions with positively charged groups (antisymmetric and symmetric -COO^- stretches give rise to broad and featureless bands around 1580 and 1400 cm^{-1}, respectively[58]). Hence, the simultaneous imprinting of the major and minor infrared spectral features upon cross-seeding of [BI] and [KR] implies that strain-specific patterns of inter-β-strand hydrogen bonding and local β-sheet twists typified by the amide I′ band's position[47,48] evoke distinct modes of packing and interactions for insulin side

dx.doi.org/10.1021/bi301144d | Biochemistry 2012, 51, 9460−9469

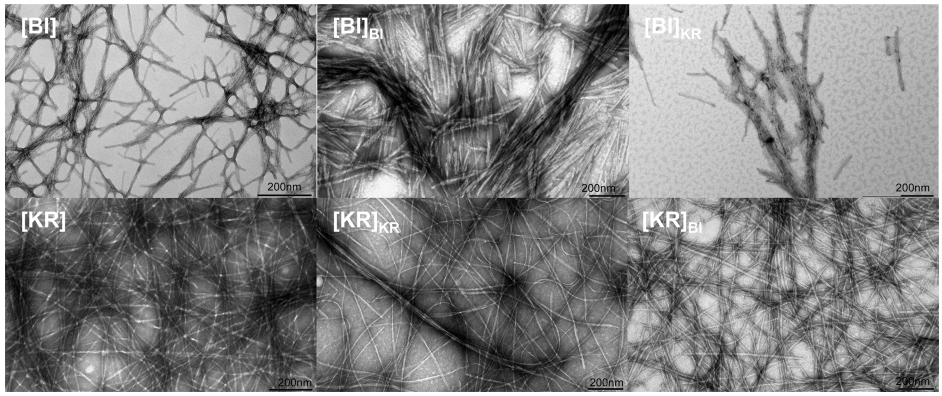

Figure 4. Negatively stained TEM images of insulin amyloid fibrils formed through spontaneous aggregation ([BI] and [KR]), seeding with homologous fibrils ($[BI]_{BI}$ and $[KR]_{KR}$), and cross-seeding ($[BI]_{KR}$ and $[KR]_{BI}$).

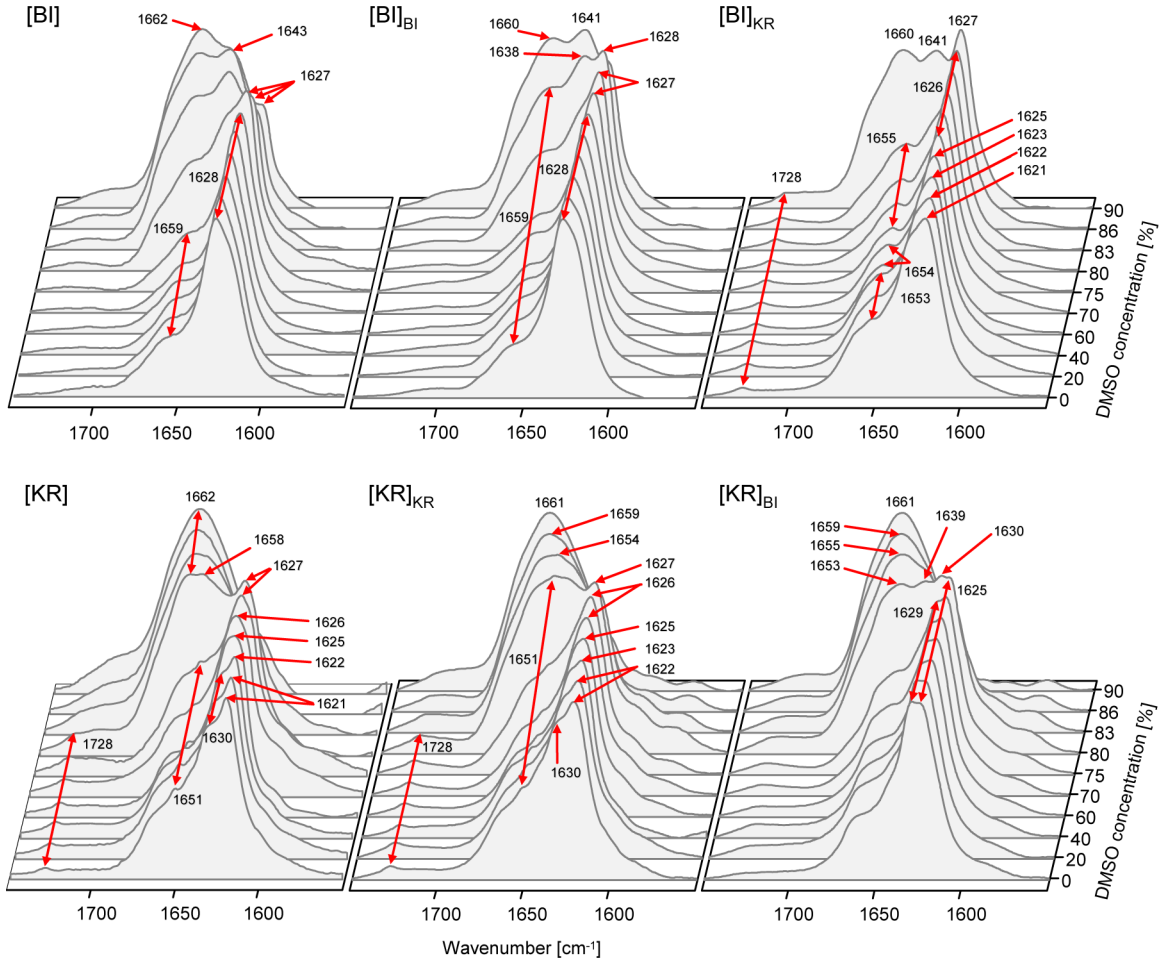

Figure 5. Gradual DMSO-induced denaturation of different types of insulin fibrils reflected in spectral changes in the amide I′ infrared band. The spectra have been collected for fibrils formed through spontaneous aggregation ([BI] and [KR]), seeding with homologous fibrils ($[BI]_{BI}$ and $[KR]_{KR}$), and cross-seeding ($[BI]_{KR}$ and $[KR]_{BI}$).

chains. We have also employed Raman spectroscopy to check whether these conformational differences affect insulin's three intramolecular disulfide bridges that are said to remain intact in amyloid fibrils.[59] Our Raman data suggest rather similar geometry and surroundings of S−S bonds regardless of the insulin amyloid type (Supporting Information).

Various amyloid strains often reveal distinct morphologies,[21,36] which prompted our interest in comparing TEM images of the different types of insulin fibrils. In Figure 4, representative TEM images of mother and daughter fibrils are presented. Although there are visible differences between amyloid aggregates formed from BI and KR molecules, there is no evidence that the memory effect controls the morphology of daughter fibrils. Regardless of the seeding history, second generations of bovine insulin fibrils tend to be shorter (100−600 nm) than corresponding KR fibrils that are often longer than 2 μm. Only mother [KR] fibrils have a broader length distribution, a likely artifact of a robust aggregation scenario

dx.doi.org/10.1021/bi301144d | *Biochemistry* 2012, 51, 9460−9469

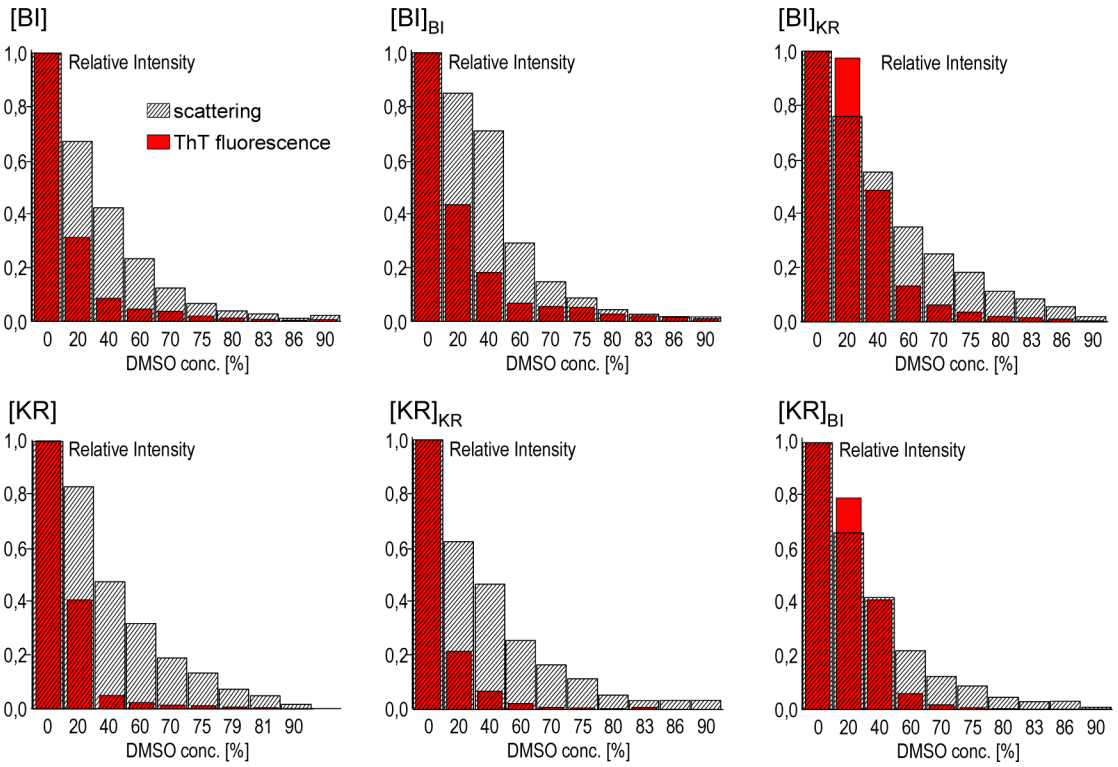

Figure 6. DMSO-induced denaturation of insulin fibrils monitored by light scattering at 350 nm and ThT fluorescence intensity at 482 nm. The data correspond to the samples and conditions used to collect the FT-IR data shown in Figure 5.

involving the rapid occurrence of high concentrations of amyloid nuclei. Another conspicuous difference between fibrils formed from BI and KR molecules is the strong tendency for lateral aggregation of the former, whereas [KR], $[KR]_{KR}$, and $[KR]_{BI}$ fibrils are singly dispersed. Still, diameters of individual protofibrils in all six types of amyloid shown in Figure 4 are similar and range between 3 and 8 nm. The strong propensity to form laterally aligned fibrils could be a consequence of the higher hydrophobicity of BI compared to that of KR. Thus, the conformational memory effect between [BI] and [KR] fibrils does not seem to affect the morphology or superstructure of amyloid fibrils, at least in a way that could be captured with TEM.

Taken together, the FT-IR and TEM data suggest that the differences between pairs of amyloid strains, $[KR]_{KR}$ versus $[KR]_{BI}$ and $[BI]_{BI}$ versus $[BI]_{KR}$, are imprinted on the secondary and tertiary structure levels of a single protofibril, rather than on the quaternary level (i.e., through different modes of association of essentially identical protofibrils). The relationship between amyloid polymorphism and the level of structural hierarchy, on which it is encoded, may vary depending on the protein aggregate (e.g., refs 29 and 46). A valuable insight into this problem may be obtained from amyloid dissection experiments that provide a gauge of the relative stability of fibrils. For example, different hamster prion strains were shown to have distinct stabilities against denaturation with guanidine hydrochloride.[68] Employing DMSO instead of guanidine is advantageous because it permits the acquisition of infrared spectra (amide I′ band), ThT fluorescence, and light scattering measurements under an identical set of sample conditions. We have shown previously that in the presence of DMSO insulin amyloid fibrils undergo a noncooperative disassembly with a dissection of quaternary structures preceding denaturation of secondary structures.[33,54] As this approach appears to be suitable for the problem of the level of amyloid structure on which the strain-specific information is stored, we have subjected the six different fibril samples to DMSO-induced disaggregation monitored with FT-IR spectroscopy, ThT fluorescence, and light scattering. Figure 5 displays stacks of infrared spectra of insulin fibrils in the presence of DMSO at a gradually increasing concentration, while Figure 6 shows the corresponding changes in ThT emission and light scattering at 350 nm. All types of fibrils undergo disassembly of the amyloidal scaffold (reflected by the decline in ThT emission) and fragmentation of fibrils (probed by light scattering intensity) at DMSO concentrations markedly lower than those required to disrupt intrafibrillar β-sheet structure. However, a more thorough analysis of spectral changes accompanying the DMSO-driven denaturation reveals intriguing details. The position of the amide I′ band remains intact at ~1628 cm^{-1} up to 80 wt % DMSO for [BI] and $[BI]_{BI}$ and up to 75%f DMSO for $[KR]_{BI}$. Only at the highest cosolvent concentration does β-sheet structure break down and do new peaks at 1643 cm^{-1} (random coil) and 1662 cm^{-1} ("DMSO-solvated random coil"[54]) emerge. On the other hand, the amide I′ band of [KR], $[KR]_{KR}$, and $[BI]_{KR}$ fibrils titrated with DMSO shifts gradually from ~1621 cm^{-1} to higher wavenumbers even at the lowest denaturant concentrations. The two ways insulin fibrils respond to DMSO-induced disaggregation ("steady" for [BI]-templated fibrils and "upshifting" for fibrils seeded with [KR]) are clearly controlled by the type of seed used to trigger daughter fibrils. Importantly, these two different "imprinted" denaturation scenarios take place under conditions of profound disruption of higher-order structures, as the data in Figure 6 indicate. The highest accessible DMSO concentrations lead to profound denatura-

dx.doi.org/10.1021/bi301144d | *Biochemistry* 2012, 51, 9460−9469

tion of elementary building blocks of amyloid fibrils and the transition of β-sheet structure to DMSO-solvated random coil (with the corresponding amide I′ position at 1662 cm^{-1}). It may be hypothesized that such tiny (perhaps of the size of the smallest oligomers or even monomers) protein particles lack the structural complexity affording kinetic traps that are necessary for different strains to coexist under identical physicochemical conditions. Hence, DMSO causes the transition from the metastable to the unstable. In other words, the completely denatured and singly dispersed protein monomers are more likely to be under thermodynamic rather than kinetic control; i.e., the conformational memory is erased, and the transient conformation reflects the free energy minimum of interactions between the insulin molecule and the solvent. Indeed, spectra of DMSO-denatured fibrils composed predominantly of KR monomers ([KR], $[KR]_{KR}$, and $[KR]_{BI}$) share a similar appearance. On the other hand, spectra of DMSO-denatured BI fibrils exhibit residual β-structure, suggesting that the distinct covalent structure of BI aggregates makes them more resistant to DMSO treatment, and that under the conditions of this study, $[BI]_{BI}$ and $[BI]_{KR}$ fibrils are not completely denatured even at the highest DMSO concentration probed. One puzzling aspect of the data shown in Figure 6 is the unusual resistance of quaternary structures of cross-seeded $[BI]_{KR}$ and $[KR]_{BI}$ against low concentrations of DMSO. Moreover, in the case of $[BI]_{KR}$, this extra stabilization appears to hold also for higher DMSO concentrations and secondary structures (Figure 5). Further studies are needed to explain mechanisms of stabilization of cross-seeded fibril variants and to assess the possible relevance of this behavior for studies on cross-species transmission of amyloid strains.

We have shown that two types of amyloid fibrils obtained from BI and KR insulins have distinct infrared features that are passed on to daughter fibrils upon cross-seeding. This closely resembles the conformational memory effect upon proliferation of amyloid strains. Also, in an analogy to strain-specific kinetics of the elongation phase in prion self-assembly,[69] we have observed variations in the kinetics of elongation of homologously seeded and cross-seeded [BI] and [KR] fibrils (Figure 2). The template-controlled intensity of ThT emission observed in this work has a parallel in the work by Cloe et al. on mutant Aβ fibrils with the capacity to cross-seed daughter fibrils with a lowered quantum yield of fluorescence of the bound stain.[55] Our FT-IR data and results of the DMSO-induced dissection of fibrils strongly suggest that structural variations underlying the strain-specific polymorphism of [BI] and [KR] fibrils are encoded on the conformational level. This agrees with the fact that no strain-specific morphological differences were observed via TEM (Figure 4).

It has been proposed that amyloid core regions with tightly packed steric zippers are particularly vulnerable to sequence modifications that would result in the emergence of new structural variants of fibrils.[14,26,49] An important finding of this study is that modifications of insulin's primary structure even outside of critical amyloidogenic regions [which for insulin have been mapped by Eisenberg et al.[49−51] (listed in Table 1)] may cause the emergence of new self-propagating amyloid strains. This statement cannot be generalized, however. For example, mutating prion protein outside of the regions responsible for critical intermolecular contacts led to amyloid fibrils with new distinct fingerprint features in the amide I′ band that nevertheless were not passed to daughter fibrils upon cross-seeding.[40] The C-terminal part of the insulin B chain is not amyloidogenic itself[50] but instead is involved in the formation of an intramolecular antiparallel β-sheet that binds together native insulin dimers. A recent study by Haas et al. suggests that the dynamics of the C-terminal part of insulin's B chain not only strongly depend on local charge distribution but also play an important part in early stages of amyloidogenesis.[66] Therefore, adding two positively charged amino acid residues, Lys and Arg, to the C-terminus is expected to have a pronounced impact on insulin dynamics. The differences in amino acid sequence between BI and KR are far from the core regions, but they can still significantly affect events on insulin amyloidogenic pathways and, in particular, interactions within the aggregation intermediate state. While structural variations related to amyloid strains may originate from core steric zippers, dynamics in remote protein parts may determine which of many accessible amyloidogenic pathways leading to different strains is taken.

■ CONCLUSIONS

Two types of insulin, BI and KR, form amyloid-like fibrils with distinct infrared features in the amide I′ band region and different morphologies. Cross-seeding of natively folded peptides with amyloid preformed from BI or KR induces daughter generations of fibrils whose infrared characteristics, but not morphology, are the same as those of the mother seed. This conformational memory effect is reminiscent of the behavior that is a hallmark of prion strains. Comparison of infrared features and DMSO denaturation profiles of mother and daughter fibrils suggests that the strain-dependent polymorphism is encoded on the level of secondary structure. Differences in the primary structure between BI and KR lie outside of the critical amyloidogenic regions of insulin but are likely to affect the dynamics of amyloidogenic intermediates leading to different amyloid strains.

■ ASSOCIATED CONTENT

Ⓢ Supporting Information

Additional Raman, FT-IR, and TEM data. This material is available free of charge via the Internet at http://pubs.acs.org.

■ AUTHOR INFORMATION

Corresponding Author

*Phone: +48 22 8220211, ext. 528. Fax: +48 22 822 5996. E-mail: wdzwolak@chem.uw.edu.pl.

Funding

This work was supported by the Polish Ministry of Education and Science (Grant NN 301 101236 to W.D.). Preparation of human recombinant insulin and its analogs was funded by the POIG Key Research Project (Contract POIG 01.01.02-00-007/08-00)

Notes

The authors declare no competing financial interest.

■ ACKNOWLEDGMENTS

The insulin samples were kindly provided by Dr. Piotr Borowicz from the Institute of Biotechnology and Antibiotics. TEM equipment was sponsored by the EU Structural Funds, Centre of Advanced Technology BIM, equipment purchase for the Laboratory of Biological and Medical Imaging (at the Nencki Institute of Experimental Biology).

■ ABBREVIATIONS

CD, circular dichroism; DMSO, dimethyl sulfoxide; FT-IR, Fourier transform infrared; GEKR, recombinant Gly^{A22}-Glu^{B3}-Lys^{B31}-Arg^{B32} human insulin analog; GKR, recombinant Gly^{A22}-Lys^{B31}-Arg^{B32} human insulin analog; GR, recombinant Gly^{A22}-Arg^{B31} human insulin analog; BI, bovine insulin; HI, human recombinant insulin; KR, recombinant Lys^{B31}-Arg^{B32} human insulin analog; TEM, transmission electron microscopy; ThT, thioflavin T; [X], spontaneously formed mother fibrils of protein X; $[X]_Y$, daughter fibrils formed upon seeding protein X with preformed fibrils of protein Y.

■ REFERENCES

(1) Chiti, F., and Dobson, C. M. (2006) Protein misfolding, functional amyloid, and human disease. *Annu. Rev. Biochem. 75*, 333−366.

(2) Fändrich, M., and Dobson, C. M. (2002) The behaviour of polyamino acids reveals an inverse side chain effect in amyloid structure formation. *EMBO J. 21*, 5682−5690.

(3) Jahn, T. R., Makin, O. S., Morris, K. L., Marshall, K. E., Tian, P., Sikorski, P., and Serpell, L. C. (2010) The common architecture of cross-β amyloid. *J. Mol. Biol. 395*, 717−727.

(4) Anfinsen, C. B. (1973) Principles that govern the folding of protein chains. *Science 181*, 223−230.

(5) Madine, J., Jack, E., Stockley, P. G., Radford, S. E., Serpell, L. C., and Middleton, D. A. (2008) Structural insights into the polymorphism of amyloid-like fibrils formed by region 20−29 of amylin revealed by solid-state NMR and X-ray fiber diffraction. *J. Am. Chem. Soc. 130*, 14990−5001.

(6) Pedersen, J. S., Andersen, C. B., and Otzen, D. E. (2010) Amyloid structure—one but not the same: The many levels of fibrillar polymorphism. *FEBS J. 277*, 4591−4601.

(7) Petkova, A. T., Leapman, R. D., Guo, Z., Yau, W. M., Mattson, M. P., and Tycko, R. (2005) Self-propagating, molecular-level polymorphism in Alzheimer's β-amyloid fibrils. *Science 307*, 262−265.

(8) Yamaguchi, K., Takahashi, S., Kawai, T., Naiki, H., and Goto, Y. (2005) Seeding-dependent propagation and maturation of amyloid fibril conformation. *J. Mol. Biol. 352*, 952−960.

(9) Dzwolak, W., Smirnovas, V., Jansen, R., and Winter, R. (2004) Insulin forms amyloid in a strain-dependent manner: An FT-IR spectroscopic study. *Protein Sci. 13*, 1927−1932.

(10) Makarava, N., and Baskakov, I. V. (2008) The same primary structure of the prion protein yields twod self-propagating states. *J. Biol. Chem. 283*, 15988−15996.

(11) Gazit, E. (2002) The "Correctly Folded" state of proteins: Is it a metastable state? *Angew. Chem., Int. Ed. 41*, 257−259.

(12) Perczel, A., Hudáky, P., and Pálfi, V. K. (2007) Dead-end street of protein folding: Thermodynamic rationale of amyloid fibril formation. *J. Am. Chem. Soc. 129*, 14959−14965.

(13) Kodali, R., and Wetzel, R. (2007) Polymorphism in the intermediates and products of amyloid assembly. *Curr. Opin. Struct. Biol. 17*, 48−57.

(14) Miller, Y., Ma, B., and Nussinov, R. (2010) Polymorphism in Alzheimer Aβ amyloid organization reflects conformational selection in a rugged energy landscape. *Chem. Rev. 110*, 4820−4838.

(15) Eichner, T., and Radford, S. E. (2011) A diversity of assembly mechanisms of a generic amyloid fold. *Mol. Cell 43*, 8−18.

(16) Fändrich, M., Meinhardt, J., and Grigorieff, N. (2009) Structural polymorphism of Alzheimer Aβ and other amyloid fibrils. *Prion 3*, 89−93.

(17) Weissmann, C., Enari, M., Klöhn, P. C., Rossi, D., and Flechsig, E. (2002) Molecular biology of prions. *Acta Neurobiol. Exp. 62*, 153−166.

(18) Peretz, D., Williamson, R. A., Legname, G., Matsunaga, Y., Vergara, J., Burton, D. R., DeArmond, S. J., Prusiner, S. B., and Scott, M. R. (2002) A change in the conformation of prions accompanies the emergence of a new prion strain. *Neuron 34*, 921−932.

(19) Aguzzi, A. (2004) Understanding the diversity of prions. *Nat. Cell Biol. 6*, 290−292.

(20) Chien, P., Weissman, J. S., and DePace, A. H. (2004) Emerging principles of conformation-based prion inheritance. *Annu. Rev. Biochem. 73*, 617−656.

(21) Diaz-Avalos, R., King, C. Y., Wall, J., Simon, M., and Caspar, D. L. (2005) Strain-specific morphologies of yeast prion amyloid fibrils. *Proc. Natl. Acad. Sci. U.S.A. 102*, 10165−10170.

(22) Ritter, C., Maddelein, M. L., Siemer, A. B., Lührs, T., Ernst, M., Meier, B. H., Saupe, S. J., and Riek, R. (2005) Correlation of structural elements and infectivity of the HET-s prion. *Nature 435*, 844−848.

(23) Tanaka, M., Collins, S. R., Toyama, B. H., and Weissman, J. S. (2006) The physical basis of how prion conformations determine strain phenotypes. *Nature 442*, 585−589.

(24) Tessier, P. M., and Lindquist, S. (2007) Prion recognition elements govern nucleation, strain specificity and species barriers. *Nature 447*, 556−561.

(25) Baskakov, L. V. (2009) Switching in amyloid structure within individual fibrils: Implication for strain adaptation, species barrier and strain classification. *FEBS Lett. 583*, 2618−2622.

(26) Surewicz, W. K., and Apostol, M. I. (2011) Prion protein and its conformational conversion: A structural perspective. *Top. Curr. Chem. 305*, 135−167.

(27) Dische, F. E., Wernstedt, C., Westermark, G. T., Westermark, P., Pepys, M. B., Rennie, J. A., Gilbey, S. G., and Watkins, P. J. (1988) Insulin as an amyloid-fibril protein at sites of repeated insulin injections in a diabetic patient. *Diabetologia 31*, 158−161.

(28) Krebs, M. R. H., MacPhee, C. E., Miller, A. F., Dunlop, I. E., Dobson, C. M., and Donald, A. M. (2004) The formation of spherulites by amyloid fibrils of bovine insulin. *Proc. Natl. Acad. Sci. U.S.A. 101*, 14420−14424.

(29) Kurouski, D., Dukor, R. K., Lu, X., Nafie, L. A., and Lednev, I. K. (2012) Normal and reversed supramolecular chirality of insulin fibrils probed by vibrational circular dichroism at the protofilament level of fibril structure. *Biophys. J. 103*, 522−531.

(30) Kurouski, D., Dukor, R. K., Lu, X., Nafie, L. A., and Lednev, I. K. (2012) Spontaneous inter-conversion of insulin fibril chirality. *Chem. Commun. 48*, 2837−2839.

(31) Foderà, V., Van De Weert, M., and Vestergaard, B. (2010) Large-scale polymorphism and auto-catalytic effect in insulin fibrillogenesis. *Soft Matter 6*, 4413−4419.

(32) Dzwolak, W., Loksztejn, A., Galinska-Rakoczy, A., Adachi, R., Goto, Y., and Rupnicki, L. (2007) Conformational indeterminism in protein misfolding: Chiral amplification on amyloidogenic pathway of insulin. *J. Am. Chem. Soc. 129*, 7517−7522.

(33) Loksztejn, A., and Dzwolak, W. (2008) Chiral bifurcation in aggregating insulin: An induced circular dichroism study. *J. Mol. Biol. 379*, 9−16.

(34) Loksztejn, A., and Dzwolak, W. (2010) Vortex-induced formation of insulin amyloid superstructures probed by time-lapse atomic force microscopy and circular dichroism spectroscopy. *J. Mol. Biol. 395*, 643−655.

(35) Nielsen, L., Frokjaer, S., Carpenter, J. F., and Brange, J. (2001) Studies of the structure of insulin fibrils by Fourier transform infrared (FTIR) spectroscopy and electron microscopy. *J. Pharm. Sci. 90*, 29−37.

(36) Dzwolak, W., Jansen, R., Smirnovas, V., Loksztejn, A., Porowski, S., and Winter, R. (2005) Template-controlled conformational patterns of insulin fibrillar self-assembly reflect history of solvation of the amyloid nuclei. *Phys. Chem. Chem. Phys. 7*, 1349−1351.

(37) Dzwolak, W., Grudzielanek, S., Smirnovas, V., Ravindra, R., Nicolini, C., Jansen, R., Loksztejn, A., Porowski, S., and Winter, R. (2005) Ethanol-perturbed amyloidogenic self-assembly of insulin: Looking for origins of amyloid strains. *Biochemistry 44*, 8948−8958.

(38) Caughey, B., Raymond, G. J., and Bessen, R. A. (1998) Strain-dependent differences in β-sheet conformations of abnormal prion protein. *J. Biol. Chem. 273*, 32230−32235.

(39) Jones, E. M., and Surewicz, W. K. (2005) Fibril conformation as the basis of species- and strain-dependent seeding specificity of mammalian prion amyloids. *Cell 121*, 63−72.
(40) Jones, E. M., Surewicz, K., and Surewicz, W. K. (2006) Role of N-terminal familial mutations in prion protein fibrillization and prion amyloid propagation in vitro. *J. Biol. Chem. 281*, 8190−8196.
(41) Pedersen, J. S., Dikov, D., Flink, J. L., Hjuler, H. A., Christiansen, G., and Otzen, D. E. (2006) The changing face of glucagon fibrillation: Structural polymorphism and conformational imprinting. *J. Mol. Biol. 355*, 501−523.
(42) Andersen, C. B., Hicks, M. R., Vetri, V., Vandahl, B., Rahbek-Nielsen, H., Thøgersen, H., Thøgersen, I. B., Enghild, J. J., Serpell, L. C., Rischel, C., and Otzen, D. E. (2010) Glucagon fibril polymorphism reflects differences in protofilament backbone structure. *J. Mol. Biol. 397*, 932−946.
(43) Ostapchenko, V. G., Sawaya, M. R., Makarava, N., Savtchenko, R., Nilsson, K. P. R., Eisenberg, D., and Baskakov, I. V. (2010) Two amyloid states of the prion protein display significantly different folding patterns. *J. Mol. Biol. 400*, 908−921.
(44) Dong, J., Wan, Z., Popov, M., Carey, P. R., and Weiss, M. A. (2003) Insulin assembly damps conformational fluctuations: Raman analysis of amide I linewidths in native states and fibrils. *J. Mol. Biol. 330*, 431−442.
(45) Huang, K., Maiti, N. C., Phillips, N. B., Carey, P. R., and Weiss, M. A. (2006) Structure-specific effects of protein topology on cross-β assembly: Studies of insulin fibrillation. *Biochemistry 45*, 10278−10293.
(46) Shashilov, V., Xu, M., Makarava, N., Savtchenko, R., Baskakov, I. V., and Lednev, I. K. (2012) Dissecting structure of prion amyloid fibrils by hydrogen-deuterium exchange ultraviolet raman spectroscopy. *J. Phys. Chem. B 116*, 7926−7930.
(47) Kubelka, J., and Keiderling, T. A. (2001) Differentiation of β-sheet-forming structures: Ab initio-based simulations of IR absorption and vibrational CD for model peptide and protein β-sheets. *J. Am. Chem. Soc. 123*, 12048−12058.
(48) Zandomeneghi, G., Krebs, M. R. H., McCammon, M. G., and Fändrich, M. (2004) FTIR reveals structural differences between native β-sheet proteins and amyloid fibrils. *Protein Sci. 13*, 3314−3321.
(49) Sawaya, M. R., Sambashivan, S., Nelson, R., Ivanova, M. I., Sievers, S. A., Apostol, M. I., Thompson, M. J., Balbirnie, M., Wiltzius, J. J., McFarlane, H. T., Madsen, A. Ř., Riekel, C., and Eisenberg, D. (2007) Atomic structures of amyloid cross-β spines reveal varied steric zippers. *Nature 447*, 453−457.
(50) Ivanova, M. I., Thompson, M. J., and Eisenberg, D. (2006) A systematic screen of β_2-microglobulin and insulin for amyloid-like segments. *Proc. Natl. Acad. Sci. U.S.A. 103*, 4079−4082.
(51) Ivanova, M. I., Sievers, S. A., Sawaya, M. R., Wall, J. S., and Eisenberg, D. (2009) Molecular basis for insulin fibril assembly. *Proc. Natl. Acad. Sci. U.S.A. 106*, 18990−18995.
(52) Silva, J. L., Silveira, C. F., Correia Junior, A., and Pontes, L. (1992) Dissociation of a native dimer to a molten globule monomer. Effects of pressure and dilution on the association equilibrium of arc repressor. *J. Mol. Biol. 223*, 545−555.
(53) Dzwolak, W., Loksztejn, A., and Smirnovas, V. (2006) New insights into the self-assembly of insulin amyloid fibrils: An H-D exchange FT-IR study. *Biochemistry 45*, 8143−8151.
(54) Loksztejn, A., and Dzwolak, W. (2009) Noncooperative dimethyl sulfoxide-induced dissection of insulin fibrils: Toward soluble building blocks of amyloid. *Biochemistry 48*, 4846−4851.
(55) Cloe, A. L., Orgel, J. P. R. O., Sachleben, J. R., Tycko, R., and Meredith, S. C. (2011) The Japanese mutant Aβ (ΔE22-Aβ(1−39)) forms fibrils instantaneously, with low-thioflavin T fluorescence: Seeding of wild-type Aβ(1−40) into atypical fibrils by ΔE22-Aβ(1−39). *Biochemistry 50*, 2026−2039.
(56) Mauro, M., Craparo, E. F., Podestà, A., Bulone, D., Carrotta, R., Martorana, V., Tiana, G., and San Biagio, P. L. (2007) Kinetics of different processes in human insulin amyloid formation. *J. Mol. Biol. 366*, 258−274.
(57) Foderà, V., Librizzi, F., Groenning, M., Van De Weert, M., and Leone, M. (2008) Secondary nucleation and accessible surface in insulin amyloid fibril formation. *J. Phys. Chem. B 112*, 3853−3858.
(58) Barth, A. (2000) The infrared absorption of amino acid side chains. *Prog. Biophys. Mol. Biol. 74*, 141−173.
(59) Kurouski, D., Washington, J., Ozbil, M., Prabhakar, R., Shekhtman, A., and Lednev, I. K. (2012) Disulfide bridges remain intact while native insulin converts into amyloid fibrils. *PLoS One 7*, No. e36989.
(60) Krebs, M. R. H., Morozova-Roche, L. A., Daniel, K., Robinson, C. V., and Dobson, C. M. (2004) Observation of sequence specificity in the seeding of protein amyloid fibrils. *Protein Sci. 13*, 1933−1938.
(61) O'Nuallain, B., Williams, A. D., Westermark, P., and Wetzel, R. (2004) Seeding specificity in amyloid growth induced by heterologous fibrils. *J. Biol. Chem. 279*, 17490−17499.
(62) Fu, X., Korenaga, T., Fu, L., Xing, Y., Guo, Z., Matsushita, T., Hosokawa, M., Naiki, H., Baba, S., Kawata, Y., Ikeda, S., Ishihara, T., Mori, M., and Higuchi, K. (2004) Induction of AApoAII amyloidosis by various heterogeneous amyloid fibrils. *FEBS Lett. 563*, 179−84.
(63) Lundmark, K., Westermark, G. T., Olsén, A., and Westermark, P. (2005) Protein fibrils in nature can enhance amyloid protein A amyloidosis in mice: Cross-seeding as a disease mechanism. *Proc. Natl. Acad. Sci. U.S.A. 102*, 6098−6102.
(64) Devlin, G. L., Knowles, T. P., Squires, A., McCammon, M. G., Gras, S. L., Nilsson, M. R., Robinson, C. V., Dobson, C. M., and MacPhee, C. E. (2006) The component polypeptide chains of bovine insulin nucleate or inhibit aggregation of the parent protein in a conformation-dependent manner. *J. Mol. Biol. 360*, 497−509.
(65) Grimsley, G. R., Scholtz, J. M., and Pace, C. N. (2009) A summary of the measured pK values of the ionizable groups in folded proteins. *Protein Sci. 18*, 247−251.
(66) Haas, J., Vöhrunger-Martinez, E., Bögenhold, A., Matthes, D., Hensen, U., Pelah, A., Abel, B., and Grubmüller, H. (2009) Primary steps of pH-dependent insulin aggregation kinetics are governed by conformational flexibility. *ChemBioChem 10*, 1816−1822.
(67) Bocian, W., Borowicz, P., Mikołajczyk, J., Sitkowski, J., Tarnowska, A., Bednarek, E., Głabski, T., Tejchman-Malecka, B., Bogiel, M., and Kozerski, L. (2008) NMR structure of biosynthetic engineered human insulin monomer B31(Lys)-B32(Arg) in water/acetonitrile solution. Comparison with the solution structure of native human insulin monomer. *Biopolymers 89*, 820−830.
(68) Peretz, D., Scott, M. R., Groth, D., Williamson, R. A., Burton, D. R., Cohen, F. E., and Prusiner, S. B. (2001) Strain-specified relative conformational stability of the scrapie prion protein. *Protein Sci. 10*, 854−863.
(69) Mulcahy, E. R., and Bessen, R. A. (2004) Strain-specific kinetics of prion protein formation in vitro and in vivo. *J. Biol. Chem. 279*, 1643−1649.